Imprinted large-scale high density polymer nanopillars for organic solar cells

Mukti Aryal and Fatih Buyukserin
Department of Electrical Engineering, University of Texas at Dallas, Richardson, Texas 75080

Kamil Mielczarek
Department of Physics, University of Texas at Dallas, Richardson, Texas 75080

Xiao-Mei Zhao
Department of Electrical Engineering, University of Texas at Dallas, Richardson, Texas 75080

Jinming Gao
Department of Chemistry, University of Texas at Dallas, Richardson, Texas 75080

Anvar Zakhidov
Department of Physics, University of Texas at Dallas, Richardson, Texas 75080

Wenchuang (Walter) Hu[a)]
Department of Electrical Engineering, University of Texas at Dallas, Richardson, Texas 75080

(Received 9 June 2008; accepted 18 August 2008; published 1 December 2008)

Nanoimprint with a large-scale nanoporous Si mold is developed to fabricate high density periodic nanopillars ($\sim 10^{10}/\mathrm{cm}^2$) in various functional polymers. A anodic alumina membrane is first obtained using electrochemical anodization. The membrane is used as a mask for a two-step plasma etching process to obtain a Si mold of 50–80 nm wide and 100–900 nm deep pores. The mold is used in nanoimprint lithography to fabricate ordered and high density polymer nanopillars and nanopores in SU-8, hydrogen silsesquixane, polymethylmethacrylate, poly(3-hexylthiophane) (P3HT), and phenyl-C61-butyric acid methyl ester (PCBM). Then, the imprinted P3HT nanopillars were used to make bulk heterojunction solar cells by depositing PCBM on top of the pillars. Imprinting provides a way to precisely control the interdigitized heterojunction morphology, leading to improved solar cell performance. © *2008 American Vacuum Society.* [DOI: 10.1116/1.2981076]

I. INTRODUCTION

Functional polymer nanostructures of controlled morphology can offer enhanced performance for various applications, such as organic photovoltaics,[1,2] light emitting diodes,[3] biosensors,[4,5] and nanomedicine.[6] Nanoimprint lithography (NIL) is a cost-effective manufacturing method to produce polymer nanostructures.[7,8] Despite the fact that NIL is a parallel printing process, mass production of nanostructures using NIL is still quite limited due to the inability of fabricating molds with high density nanostructures over large areas. Conventional mold fabrication techniques, such as e-beam lithography (EBL) and photolithography, are impractical to pattern nanostructures over large scale because of their slow speed and/or high cost. Here, we present a cost-effective method that combines electrochemical process and high density plasma etching to make Si molds of dense and ordered nanopores over large area. Using the nanoporous Si mold, high density ($\sim 10^{10}/\mathrm{cm}^2$) nanostructures in various polymer systems are produced using both thermal and UV nanoimprint lithography.

II. FABRICATION OF NANOPOROUS SI MOLDS

Figure 1 shows the schematic of the mold fabrication and NIL processes. Freestanding nanoporous anodic alumina membranes (AAMs) are first formed using electrochemical anodization and voltage reduction method. The membrane is then used as a mask to etch a Si substrate using a two-step inductively coupled plasma (ICP) etching process. Ar plasma is first used to remove the rough barrier side of the AAM [Fig. 1(b)], followed by Si etching using Cl_2 plasma [Fig. 1(c)]. After etching, the AAM is removed from the Si mold, which is then treated with antiadhesion perfluorodecyltrichlorosilane. Fabrication of high density and ordered polymer nanopillars of well-controlled morphology is then demonstrated using thermal and/or UV nanoimprint lithography [Figs. 1(d) and 1(e)].

Nanoporous anodic alumina or aluminum oxide (AAO) has been under extensive investigation during the past decades for various applications, such as biosensing, filtering, photonic crystal, magnetic recording media, and patterning.[5,9–11] Good control of pore ordering and uniformity has been achieved using two-step anodization and/or prepatterned aluminum induced anodization.[12,13] It has been reported that using voltage reduction method during anodization can generate an alumina branching layer, which can be dissolved to obtain freestanding AAO membranes or AAM.[14] For some of these applications, nanoporous structures of AAO were transferred into other materials using additive deposition and/or etching methods.[12,15–19] Our initial experiments indicated that direct two-step anodization of evaporated thin Al film on Si cannot produce uniform and ordered

[a)]Electronic mail: walter.hu@utdallas.edu

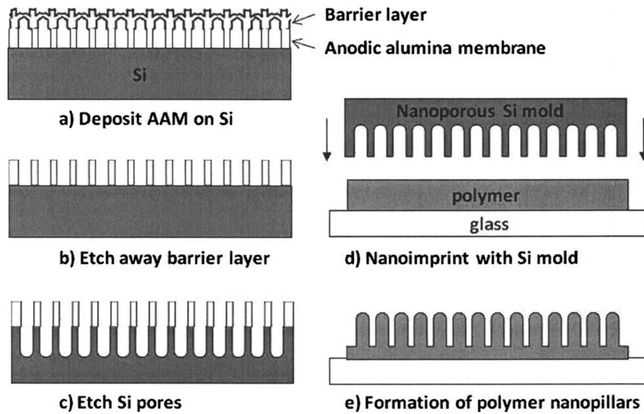

FIG. 1. Schematic of the Si mold fabrication and NIL process to make high density polymer nanopillars over large areas. (a) Placing a freestanding anodic alumina membrane on top of a Si substrate. (b) Ar plasma etching to remove the rough barrier layer of the AAM. (c) Cl_2 and Ar plasma etching to create Si nanopores using AAM as a mask. (d) After AAM removal, the perfluorodecyltrichlorosilane treated Si mold is used for nanoimprint lithography. (e) Formation of polymer nanopillars after releasing the Si mold from the substrate.

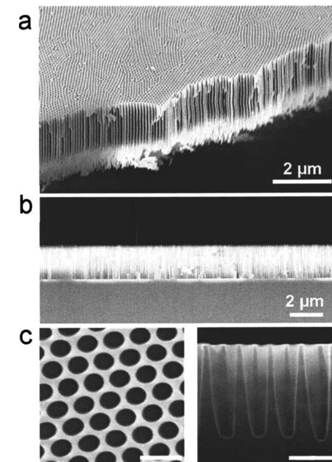

FIG. 2. SEM images of (a) a freestanding anodic alumina membrane; (b) cross section of AAM on Si after removal of the barrier layer; (c) top view and cross-sectional view of the nanoporous Si mold after the second plasma etching and removal of AAM (scale bar is 200 nm).

nanopores due to limited Al thickness. Therefore in this study, we have developed the transfer of anodic Al membrane onto a Si wafer surface for nanoimprinting applications. Various techniques have been developed to improve the adhesion between the AAM and Si, to reduce defect densities, to remove the rough AAM barrier layer, and to obtain high-aspect ratio Si nanopores using high density plasma etching with gradually varied plasma pressure.

Aluminum plates were mechanically polished using a set of alumina lapping films with particle size gradually from 30 to 1 μm. The plates were then annealed under nitrogen atmosphere at 500 °C for an hour to release stress and to increase grain sizes. Electrochemical polishing in a solution of H_3PO_4:H_2SO_4 (9:1) with CrO_3 (20 gm/l) was used to obtain low surface roughness (~3 nm) of the plates. The first step anodization was performed in 0.3*M* oxalic acid with 50 V bias voltage at 8 °C for 10–20 h. The film was dissolved in a solution of 0.2*M* CrO_3 and 0.4*M* H_3PO_4. The second anodization was performed at similar conditions at 50 V for 10 min, followed by reduction in voltage (decrease 5% of the present value in every 2 min) until 15 V. During such process, the nanopores become smaller, branch out, and form a thin barrier layer.[20] After the voltage reduction, the thin Al_2O_3 barrier layer at the interface of AAM and the remaining Al plate were partially dissolved in 10 wt % H_3PO_4 solution. AAM of 1–2 in.^{2} areas was detached from the Al plate. Figure 2(a) shows a scanning electron microscopy (SEM) image of a freestanding AAM. The AAM contains uniform pores of 50–60 nm in diameter and 2–3 μm in length. The top surface of the AAM is very smooth, while the back side of the AAM is the rough barrier layer.

The direct use of freestanding AAM as an etch mask has two problems. First, it is hard to transfer large pieces of the thin and brittle AAMs onto Si with conformal contact. Second, the barrier layer of AAM resulted from the voltage reduction process is very rough and blocks the nanopores and Si from plasma etching. For good AAM attachment on the Si substrates, a solvent-assisted AAM attachment process was used. A few drops of solvent, e.g., isopropyl alcohol, were cast over the AAM immediately after the membrane was placed on the Si surface. The solvent spreads quickly over the entire contact area between the membrane and Si, removing the air at the interface. The surface tension of the solvent during the spreading generates capillary forces to pull the membrane toward Si, thus results in a uniform contact between the two surfaces. After the solvent was dried, the AAM remains attached to the Si substrate due to van der Waals and Coulomb forces.[21] We have noticed the presence of static charges in the AAM after the electrochemical process, which sometimes made the membrane strongly attached to the container walls. However, even with the solvent-assisted attachment, there were still microscale voids between the AAM and Si, as revealed by SEM imaging (not shown). The conformal contact of AAM with Si substrate was further improved during the first plasma etching [Fig. 1(b)], where electrostatic forces between the Si and AAM (due to substrate bias and ion bombardment) generate conformal attachment and eliminate the microscale voids.

The AAM was placed on Si with the rough barrier side facing up. For good pattern transfer from the AAM to Si, an Ar plasma etching process (ICP power of 300 W, rf bias power of 200 W, and pressure of 10 mTorr) was used for 10 min to remove the rough barrier layer, yielding uniform AAM pores and reducing the thickness of the AAM, as shown in Fig. 2(b). It was observed that conformal contact between the AAM and Si was achieved after the first etching step. The attachment of freestanding AAM on Si was found to be similar to the direct-grown AAM from thin Al film deposited on Si.[18] However, the pore ordering and uniformity are better since a two-step anodization was used to prepare the AAM. Another benefit of the etching process is that it allows us to use thicker AAM (>3 μm) so that we can handle bigger AAM sample easily. The second etch step was

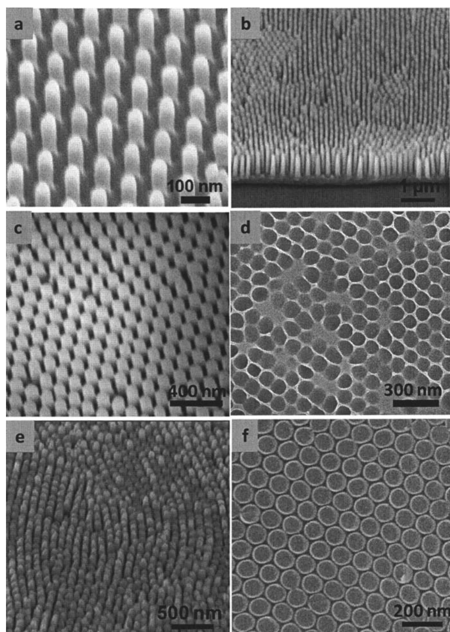

FIG. 3. 45° tilted SEM images of (a) 150 nm and (b) 600 nm tall SU-8 pillars; (c) 150 nm tall HSQ pillars; (d) 80 nm PMMA pores with 20 nm wall thickness formed by imprint with HSQ pillar molds as shown in (c); (e) ~80 nm tall P3HT, and (f) 70 nm tall PCBM pillars.

used to transfer AAM structures into underneath Si using Ar:Cl_2 (1:1) plasma at the ICP power of 300 W, rf bias power of 200 W, and consecutive pressures of 5, 10, 15 mTorr for 3 min for each step to achieve uniform pore profile and high aspect ratio. Increasing plasma pressure gradually when the pores get deeper is necessary to maintain a uniform lateral Si etching rate along the pore depth. SEM images in Fig. 2(c) show the top view and cross-sectional view of the etched Si nanopores. Pores of uniform diameter (80 nm), spacing (20 nm), controllable depth (200–900 nm), and cylindrical profiles were obtained. These dimensions can be controlled by adjusting the plasma pressure, ICP and bias power, and Cl_2 and Ar ratio. After the etching, the AAM was removed using a tape and the porous Si mold was cleaned in a piranha solution for 30 min. The Si mold was then soaked in 1%–2% perfluorodecyltrichlorosilane or $CF_3-(CF_2)_7-(CH_2)_2-SiCl_3$ in *n*-heptane for 5 min, dried in N_2, and baked at 100 °C for 10 min. Such treatment resulted in a superhydrophobic mold with surface energy of 17 mJ/m^2 for successful demolding.

III. NANOIMPRINT OF POLYMER NANOPILLARS AND NANOPORES

Both thermal and UV nanoimprint processes using these nanoporous Si molds were carried out on an Obducat 2.5 nanoimprinter to produce nanopillars or nanopores in various polymer materials over large scale (1–2 $in.^2$), as shown in Fig. 3. For UV nanoimprint, SU-8 was spin coated on a glass substrate and it was UV cured after nanoimprinting. The SU-8 pillar height can be precisely controlled by adjusting imprint temperature, pressure, and time. Figures 3(a) and 3(b) show tilted SEM views of 150 and 600 nm tall SU-8 nanopillars of uniform 50–80 nm diameter, respectively. Nanoimprint lithography was done at a pressure of 5 MPa and a temperature of 100 °C for 5–15 min. Figure 3(c) shows 150 nm tall hydrogen silsesquioxane (HSQ) pillars imprinted at a temperature of 180 °C and a pressure of 5 MPa for 3 min. The HSQ was then cured under O_2 plasma exposure (50 mTorr and 50 W bias power) for 10 min, followed by thermal annealing at 700 °C in oxygen for an hour. Using the imprinted HSQ pillars as a mold, polymethylmethacrylate (PMMA) nanopores of 80 nm diameter and 20 nm wall thickness were formed by thermal NIL, as shown in Fig. 3(d). Moreover, these Si molds were used to imprint regioregular poly-3-hexylthiophene (P3HT) and [6-6]-phenyl-butyric acid methylester (PCBM) nanostructures for organic solar cells. Figure 3(e) shows 80 nm wide pillars imprinted at 120 °C and 5 MPa for 10 min on a 60 nm thick P3HT film. The selection of the NIL conditions is strongly related to the glass transition temperature (T_g) and physical properties of the polymer used. Typically, 20–50 °C above the T_g of the polymer was chosen to obtain reasonable low viscosity to fill the Si pores. Direct imprinting in inorganic PCBM film was also performed under a pressure of 5 MPa and a temperature of 180 °C for 5 min. 70 nm tall PCBM pillars have been fabricated, as shown in Fig. 3(f). The demonstrated imprint process to form these P3HT and PCBM nanostructures provides an effective method to precisely control the heterojunction morphology of vertical alignment and lateral periodicity for organic photovoltaic devices. The polymer nanopillars can be also used as tubular particles for nanomedicine applications, where therapeutic and diagnostic molecular agents can be encapsulated in the polymer composites. Application in nanomedicine will be discussed elsewhere.

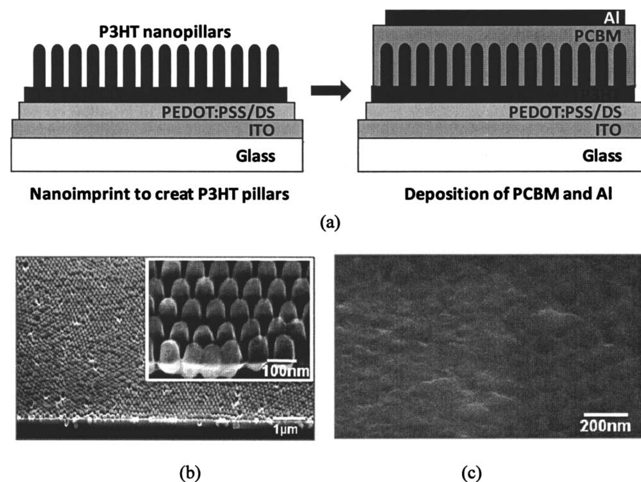

FIG. 4. (a) Schematic of solar cell fabrication process; [(b) and (c)] 45° tilted SEM view of P3HT pillars.

IV. FABRICATION AND CHARACTERIZATION OF ORGANIC SOLAR CELLS

As shown in Fig. 4, bipolar heterojunction (BHJ) organic

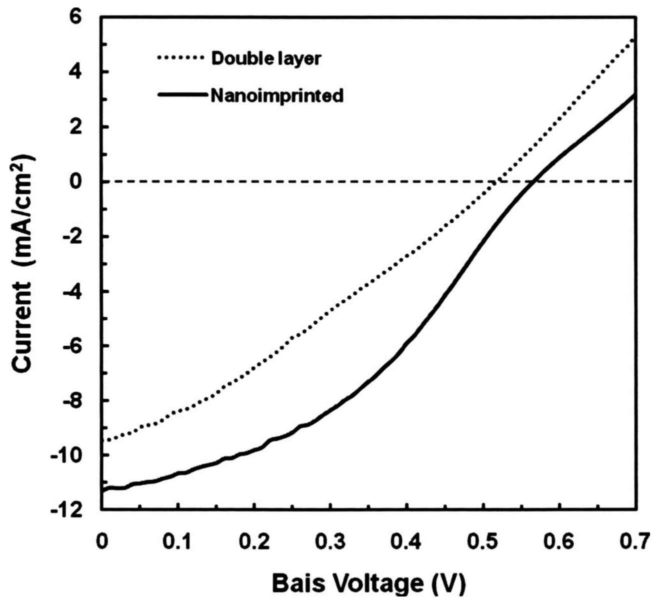

FIG. 5. *I-V* curves of organic solar cells for both bilayer and imprinted nanopillar devices.

solar cells were fabricated using imprinted P3HT nanopillars. First, the hole conducting polymer, poly (3,4-ethylenedioxythiophene)-polystyrene sulphonic acid or PEDOT:PSS or poly(3,4-ethylenedioxythiophene)/Poly(styrenesulfonate) (H. C. Starck, Inc.) mixed with D-sorbitol (Aldrich) was spin coated on indium tin oxide coated glass (Sigma Aldrich) substrates as a buffer layer and dried in N_2 at 150 °C for 60 min. Then, the 1.5 wt % solution of P3HT (Reike Metal, Ltd.) in chlorobenzene was spin casted on top of the buffer layer. The samples were stored for 12 h in a dry box. Nanopillar structures of P3HT were formed by nanoimprinting using the nanoporous Si mold and similar nanoimprinting condition described above [Fig. 3(e)]. After the formation of nanopillar structures, 0.8 wt % of PCBM on dichloromethane was spin casted as electron transfer material. Dichloromethane was chosen as a solvent because it dissolves PCBM well but not P3HT, allowing stacking PCBM on top of P3HT layer. Figures 4(b) and 4(c) show 45° tilted SEM views of the device cross sections before and after PCBM deposition, showing that a relatively uniform PCBM deposition is successful. After PCBM spin casting, the samples were baked on a hotplate in N_2 at 60 °C for 10 min to remove solvent. A 100-nm-thick aluminum was thermally evaporated on the PCBM coated sample as the top electrode.

As a control study, similar process was used to fabricate double layer nonpatterned solar cells without the imprint process. The bilayer devices contain 50 nm PCBM on 50 nm P3HT. These devices were measured using Air Mass 1.5 solar simulated light (AM 1.5) at 100 mW/cm^2. The *I-V* curves of nanoimprinted and nonpatterned devices are shown in Fig. 5. The open circuit voltage (V_{oc}), short circuit current density (J_{sc}), fill factor (FF), and efficiency (η) of these devices were listed in Table I. The solar cell built on imprinted P3HT pillars show improved performance (78% increase in power conversion efficiency, 38% increase in fill factor, and

TABLE I. Device characteristics for bilayer unimprinted and imprinted solar cells.

Parameters	Bilayer	Nanoimprinted
V_{oc} (V)	0.52	0.57
J_{sc} (mA/cm^2)	9.4	11.3
Fill factor (FF)	0.29	0.40
Efficiency η (%)	1.44	2.57

20% increase in short circuit current) over the nonpatterned one. We believe the major reason is because the well-controlled interdigitized heterojunction morphology allows more efficient exciton dissociation and charge transport, as suggested by several theoretical studies.[22,23] Ongoing research is underway to investigate several devices issues, e.g., PCBM filling of P3HT pillars, effects of pillar height, pitch, and stability to further improve solar cell performance.

V. CONCLUSIONS

In summary, nanoporous Si molds were produced by inductively coupled plasma etching using freestanding anodic alumina membranes as etch mask. Solvent and plasma assisted attachment results in conformal contact of the AAM on the Si substrate over large areas. Si molds of high density ($\sim 10^{10}$ pores/cm^2) nanopores of uniform size, depth, and profile have been successfully made. The diameter and interpore distance or the pitch of the pores in AAM can be controlled by varying anodization conditions such as the applied voltage, electrolyte type, and temperature. Pore depth and profile can be controlled by adjusting the plasma etching conditions, e.g., Cl_2:Ar ratio, pressure, bias power, and time. Using these Si molds in nanoimprint lithography, ordered and dense polymer nanopillars and nanopores in SU-8, HSQ, PMMA, P3HT, and PCBM have been fabricated over 1–2 in.^{2} areas. Then, the imprinted P3HT nanopillars were used to make bulk heterojunction solar cells by depositing PCBM on top of the pillars. Imprinting provides a way to precisely control the interdigitized heterojunction morphology, leading to improved solar cell performance.

ACKNOWLEDGMENTS

This work is partially funded by the Mouncrief Foundation, Dallas, Texas and by the Air Force Office of Scientific Research through the SPRING program (No. FA9550-06-1-0403).

[1]F. A. Boroumand, P. W. Fry, and D. G. Lidzey, Nano Lett. **5**, 67 (2005).
[2]M. S. Kim, J. S. Kim, J. C. Cho, M. Shtein, L. J. Guo, and J. Kim, Appl. Phys. Lett. **90**, 123113 (2007).
[3]H. Yamamoto, J. Wilkinson, J. P. Long, K. Bussman, J. A. Christodoulides, and Z. H. Kafafi, Nano Lett. **5**, 2485 (2005).
[4]Y. Lu and S. C. Chen, Adv. Drug Delivery Rev. **56**, 1621 (2004).
[5]I. Vlassiouk, A. Krasnoslobodtsev, S. Smirnov, and M. Germann, Langmuir **20**, 9913 (2004).
[6]J. P. Rolland, B. W. Maynor, L. E. Euliss, A. E. Exner, G. M. Denison, and J. M. DeSimone, J. Am. Chem. Soc. **127**, 10096 (2005).
[7]S. Y. Chou, P. R. Krauss, and P. J. Renstrom, Appl. Phys. Lett. **67**, 3114 (1995).

[8]L. J. Guo, Adv. Mater. (Weinheim, Ger.) **19**, 495 (2007).
[9]S. Bandyopadhyay, Phys. Rev. B **61**, 13813 (2000).
[10]H. Masuda, M. Ohya, K. Nishio, H. Asoh, M. Nohtomi, A. Yokoo, and T. Tamamura, Jpn. J. Appl. Phys. **39**, 1039 (2000).
[11]G. C. Wood and J. P. O'Sullivan, Electrochim. Acta **15**, 1865 (1970).
[12]H. Masuda and K. Fukuda, Science **268**, 1466 (1995).
[13]H. Masuda, H. Yamada, M. Satoh, H. Asoh, M. Nakao, and T. Tamamura, Appl. Phys. Lett. **71**, 2770 (1997).
[14]R. C. Furneaux, W. R. Rigby, and A. P. Davidson, Nature (London) **337**, 147 (1989).
[15]M. C. Kang, S. F. Yu, N. C. Li, and C. R. Martin, Langmuir **21**, 8429 (2005).
[16]J. Y. Liang, H. L. Luo, R. Beresford, and J. Xu, Appl. Phys. Lett. **85**, 5974 (2004).
[17]H. Masuda, A. Abe, M. Nakao, A. Yokoo, T. Tamamura, and K. Nishio, Adv. Mater. (Weinheim, Ger.) **15**, 161 (2003).
[18]D. Crouse, Y. H. Lo, A. E. Miller, and M. Crouse, Appl. Phys. Lett. **76**, 49 (2000).
[19]Y. D. Wang, S. J. Chua, M. S. Sander, P. Chen, S. Tripathy, and C. G. Fonstad, Appl. Phys. Lett. **85**, 816 (2004).
[20]G. W. Meng, Y. J. Jung, A. Y. Cao, R. Vajtai, and P. M. Ajayan, Proc. Natl. Acad. Sci. U.S.A. **102**, 7074 (2005).
[21]Y. D. Wang, K. Y. Zang, and S. J. Chua, J. Appl. Phys. **100**, 54306 (2006).
[22]C. M. Maritn, V. M. Burlakov, H. E. Assender, and D. A. R. Barkhouse, J. Appl. Phys. **102**, 104506 (2007).
[23]P. K. Watkins, A. B. Walker, and G. L. B. Verschoor, Nano Lett. **5**, 1814 (2005).